Automatic Classification of Erythrocytes Using Artificial Neural Networks and Integral Geometry-Based Functions

Yaima Paz-Soto*, Silena Herold-Garcia†, Leandro A. F. Fernandes‡ and Saul Díaz-Matos†
* Engineering and Thecnical Science Faculty
Universidad de Guántanamo, Guántanamo, Cuba
Email: ysoto@cug.co.cu
† Universidad de Oriente, Santiago de Cuba, Cuba
Email: silena@uo.edu.cu, saul.diaz@estudiantes.uo.edu.cu
‡ Universidade Federal Fluminense, Niterói, Brazil
Email: laffernades@ic.uff.br

***Abstract*—The red blood cell deformation caused by disorders like sickle cell disease can be assessed by observing blood samples under a microscope. This manual process is cumbersome and prone to errors but can be supported by automated techniques that allow red blood cells to be classified according to the shape they present. There are proposals in the literature that use functions based on integral geometry to obtain a description of the cells' contour before performing classification, reaching 96.16% accuracy with the use of the k-Nearest Neighbor (KNN) classifier. In those approaches, the classification-confusion cases persist mainly in the classes of most significant interest, which are those related to the detection of deformed cells. In this work, we use artificial neural networks-based classifiers, trained with the characteristics obtained from integral geometry-based functions, to classify erythrocytes into *normal*, *sickle*, and *other deformations* classes. Our proposal achieves accuracy of 98.40%. This result is superior to those of previous studies concerning the classes of greatest interest. Also, our approach is computationally more efficient than previous works, making it suitable for supporting medical follow-up diagnosis of sickle cell disease.**

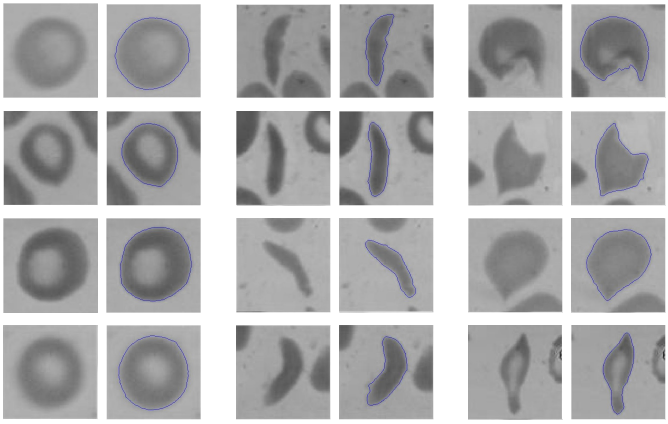

Fig. 1. Examples of erythrocytes with normal shape (left), sickle shape (center), and other deformations (right). The contours are highlighted in blue. Note that in some cases, cells with other deformations are similar to normal cells or sickle cells (*e.g.,* lines three and four in the right columns).

I. Introduction

Sickle cell anemia is a hemoglobinopathy that causes deformation of red blood cells, which lose elasticity and acquire a sickle or crescent appearance (Fig. 1, center and right columns). Red blood cell deformation and rigidity can cause vascular obstructions, generating intense crises of pain in the joints and even heart attacks [1]. According to the World Health Organization (WHO), approximately 5% of the world's population carries trait genes for hemoglobin disorders, mainly sickle-cell disease and thalassemia. In countries such as Cameroon, Republic of Congo, Gabon, Ghana, and Nigeria, the prevalence is between 20% to 30%, while in some parts of Uganda, it is as high as 45% [2]. Sickle cell anemia is the most common hereditary disease in Cuba. On average, 3% of Cubans is a carrier of this severe hemolytic anemia [3]. It is estimated that about 8% of Afro-descendants in Brazil have sickle cell anemia [4].

Clinical follow-ups of patients affected with sickle cell anemia consist of carrying out complementary tests, which include observing peripheral blood samples under a microscope to obtain a criterion about the deformation of the red blood cells. This process is quite cumbersome and prone to errors since the specialist visually evaluates the cellular deformation, with the consequent margin of error introduced by his/her implicit subjectivity and the variability of the criteria in terms of the deformation of the cell.

In practice, it has been observed that the use of automated methods for the classification of erythrocytes as having or not some deformation allows obtaining reliable results in a relatively short period compared to the manual process. But it is important to notice that the automatic process is highly dependent on the set of characteristics used to represent the contour of the cells to be studied, which allows to obtain a valid criterion on their shape efficiently. Two main approaches for employing characteristics for shape description exist: (i) the use of elemental shape characteristics directly obtained from the contour, such as circular and elliptical shape

coefficients, roundness, eccentricity, perimeter, area, diameter, among others; and (ii) the use of characteristics obtained from the functional representation of the contour, a variant with advantages regarding the possibility of using a better description of complex shapes.

For the first approach, recent proposals report high accuracy values ranging from 94.56% to 99.94% using different classifiers and considering different sets of classes for red blood cells' shape. For instance, Abood *et al.* [5] (98%), Safca *et al.* [6] (96%) and Delgado-Font *et al.* [7] (95%) used Linear Discriminant Analysis (LDA). Chy and Rahaman [8] (95%) and Alkrimi *et al.* [9] (98%) employed Support Vector Machine (SVM) classifiers, while Alkrimi *et al.* [9] (98%), Alom *et al.* [10] (99.94%), Grochowskiet *et al.* [11] (94.56%), Elsalamony [12] (95%) and Tyas *et al.* [13] (95%) explored the power of Neural Networks. For the second approach, there are some characteristics obtained from the functional representation of the contour of shapes that report accuracy values ranging from 84% to 96.16%. Examples include the UNL-Fourier transform using LDA with template matching, as proposed by Frejlichowski [14] (92.48%) and the curvature as a function of the contour arc length using Hidden Markov Models (HMM), as developed by Delgado-Font *et al.* [15] (84%). Special attention is given to shape descriptors derived from integral geometry-based functions (*e.g.,* Gual-Arnau *et al.* [16], 96.16%, and Herold-Garcia and Fernandes [17], 94.7%) and the representation of the contour on the shape space with elastic metrics (*e.g.,* Gual-Arnau *et al.* [18], 93.33%, and Epifanio *et al.* [19], 94%), both using the *k*-Nearest Neighbor (KNN) algorithm for supervised classification.

In the process of classifying erythrocytes according to their shape, each class consists of elements that are representative of the shape studied, be it a normal cell, sickle cell or a cell with another deformation. The potential of the functions as descriptors have been demonstrated on cases where cells from different classes have similar shapes. For instance, see the last two examples of cells with other deformations in Fig. 1 and notice that they are challenging cases because they are similar to, respectively, normal and sickle cells. Results showed that the functional representations proposed by Gual-Arnau *et al.* [16] and Herold-Garcia and Fernandes [17] are more effective than the use of elemental characteristics on challenging cases, where the performance achieved using elemental features was less than 80% [16] as this kind of feature is not suitable under these conditions.

On the one hand, the use of elemental shape characteristics (the first approach) with classifiers based on neural networks reports good accuracy using data from classes with objects that are representative of each studied deformation and well-differentiated between them. On the other hand, integral geometry-based solutions (the second approach) seems to describe the geometry of erythrocytes better, but the use of simple classifiers such as KNN limits their power.

In this work, we propose the use of integral geometry-based characteristics together with neural networks to classify erythrocytes as *normal*, *sickle* or *other deformations*. The aim is improving the classification performance by taking advantage of what this kind of descriptor and neural network-based classifiers have to offer best, especially for the classes of greater interest (*i.e., sickle* and *other deformations*) and on cases where confusion persist due to shape similarities.

The main contribution of this paper is the use of Artificial Neural Networks (ANN) trained with features obtained using integral geometry-based functions to perform the morphological analysis and classification of red blood cells. In this paper, we have considered the weighted integrated generalized support function [16], the Crofton descriptor [16], and three computationally-efficient variants of those [16], [17] as input data to the ANN-based classifier. Our approach's performance is superior to state-of-the-art proposals, and the better results are obtained with one of the descriptors that guarantee the reduction of computational cost.

II. Material and Methods

Fig. 2 illustrates the workflow of the proposed approach, which consists of the following steps:

1. To obtain the contour of previously segmented erythrocytes. In our experiments, we have used an image database that provides contours extracted using the level-set method (see Section III-A).
2. To obtain the representation of the shape of erythrocytes as integral geometry-based feature vectors.
3. To perform erythrocytes supervised classification, by training and evaluating artificial neural network models with the characteristics obtained in the second step.

In the following sections, we first present the two classic integral geometry-based functions used to represent the contour of objects (Section II-A), and then we describe three efficient approximations for those functions (Section II-B). The feature vectors computed from those five solutions (Section II-C) are used (individually) as input to the ANN responsible for classifying a given erythrocyte with respect to its shape (Section II-D). Section II-E discusses the computational cost of the descriptors and the computational complexity of classifiers.

A. Classic Integral Geometry-Based Functions

Let $\text{int}(D)$ be the interior of a compact domain D (*i.e.,* the erythrocyte) and L_1^2 a straight line in $\mathbb{R}^2$ given by the normal equation of the line, $x\cos(\phi)+y\sin(\phi)=p$, where $(x,y)\in\mathbb{R}^2$, ϕ is the angle between the x-axis and the normal to the line and p is the distance from the origin O of $\mathbb{R}^2$ (taken as the centroid of D) to the line. Taking the length $\left|L_1^2\cap\text{int}(D)\right|\geq 0$ and the angle $\phi\in[0^\circ,360^\circ)$, the generalized support function of D is [20]:

$$p(\sigma,\phi)=\begin{cases}\sup_{L_1^2}\left\{p \mid \left|L_1^2\cap\text{int}(D)\right|\geq\sigma\right\} & , \sigma\leq\sigma_M(\phi)\\ 0 & , \text{otherwise}\end{cases} \quad (1)$$

where sup denotes the supremum and $\sigma_M(\phi)$ is the major length σ of $|L_1^2\cap\text{int}(D)|$ for a given ϕ-value.

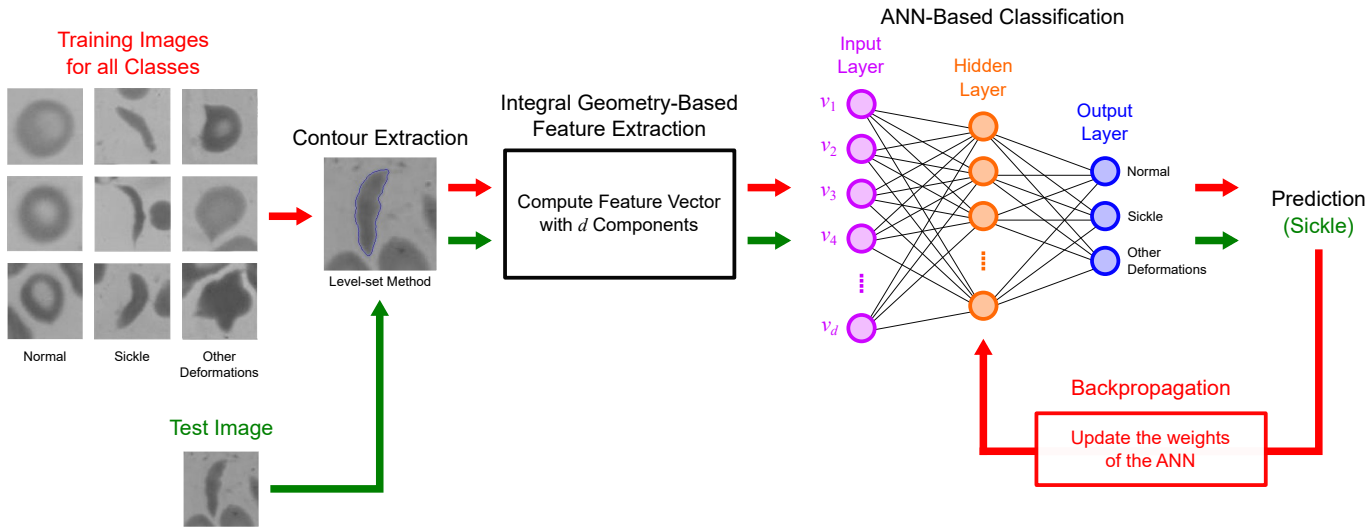

Fig. 2. The steps of the proposed approach for erythrocyte classification according to their shape. Red denotes the workflow for training of the proposed model. Green indicates the workflow for classifying a given test image.

The weighted integrated generalized support function (2) proposes integration with respect to σ for (1), so it depends on one parameter, the angle ϕ, and is defined as follows [20]:

$$W(\phi) = \frac{\sigma_M(\phi)}{\sigma_M} \int_0^{\sigma_M(\phi)} p(\sigma,\phi)\, d\sigma, \tag{2}$$

where σ_M is the largest value of all the $\sigma_M(\phi)$ existing in the representation.

Both functions (1) and (2) were presented by Gual *et al.* [20] as shape descriptors. In this work, we only use (2) because of its superior performance in comparison to (1) in previous experiments. Please, refer to [16], [17], [20] for details.

Now, let:

$$\sigma(p,\phi) = \left| L_1^2 \cap D \right| \tag{3}$$

be the length of the intersection of L_1^2 with D. This function was used by Gual-Arnau *et al.* [16] as the base for the Crofton's descriptor:

$$C_\rho(\phi) = \int_0^{\rho} \sigma(p,\phi)\, dp, \tag{4}$$

where $\rho \in [0, p(\phi)]$ is a user-defined parameter, and $p(\phi) = \sup_{L_1^2} \left\{ p \mid L_1^2 \cap D \neq \emptyset \right\}$ is the support function of D.

B. Efficient Approximations of Integral Geometry-Based Functions

Considering that the most relevant information of any region is found mainly in the area close to its contours, Gual *et al.* [20] developed a "cut" version of $W(\phi)$ (2) as follows:

$$W_c(\phi) = \int_0^{\sigma_0} p(\sigma,\phi)\, d\sigma, \tag{5}$$

where $\sigma_0 < \sigma$. The $W_c(\phi)$ function considers for integration only the portion of σ values closest to the region's border. $W_c(\phi)$ is the first function proposed to reduce the computational cost of integral geometry-based descriptors.

Recently, Herold-Garcia and Fernandes [17] proposed two new descriptor functions for erythrocyte shape classification inspired on previous integral geometry-based solutions, but with significantly less computational effort: $\sim 98\%$ less computation. Those descriptors are defined as:

$$p_\Phi(\sigma,\phi) = \{ p(\sigma,\phi) \mid \phi \in \Phi) \} \tag{6}$$

and

$$\sigma_\Phi(p,\phi) = \{ \sigma(p,\phi) \mid \phi \in \Phi \}, \tag{7}$$

where

$$\Phi = \left\{ \phi_0 + \frac{i-1}{n} 360^\circ \mod 360^\circ \right\}_{i=1}^{n} \tag{8}$$

is a discrete set of n equally spaced angular values such that $0^\circ \leq \phi_1 < \cdots < \phi_n < 360^\circ$, and $\phi_0 \geq 0^\circ$ is a constant.

C. Feature Vectors

As proposed in the original works, the feature vectors for the one-dimensional functions (2), (4) and (5) are composed of the magnitude of the 2nd to the 6th coefficients of the Fourier approximations for the one-dimensional vector obtained with these function, directly considering each vector as a one-dimensional discrete signal (see [16], [20] for details). For (6) and (7), it is taken as descriptor the magnitude of the 2nd to the 6th coefficients of the Fourier approximations of the signals formed by stacking the values computed evaluating the functions for the angles in Φ, as described in [17]. Invariance to rotation and scaling in all cases is achieved by normalizing the feature vectors by the magnitude of the 1st Fourier coefficient. Thus, the i^{th} component of the feature vector $v = (v_1, v_2, \cdots, v_d)$ is given by:

$$v_i = \left\| \frac{\mathscr{F}_{i+1}}{\mathscr{F}_1} \right\|, \tag{9}$$

where $\mathscr{F}_j$ denotes the j^{th} coefficient of the Fourier approximation of the discrete signal computed using (2), (4), (5), (6), or (7), and $\|z\|$ denotes the magnitude of a complex number z.

D. ANN-Based Classifier

An ANN is a supervised learning algorithm that, from a set of input data of dimension d called input vector, computes an output vector having m dimensions, using a function f modeled by intermediate layers of nodes (or neurons) placed between the input and the output layer.

In this work, we consider an ANN having three fully connected layers (see Fig. 2): the input layer including d nodes, one hidden layer having h neurons, and the output layer with $m = 3$ neurons, one for each class of shape: *normal*, *sickle*, and *other deformations*. Each node in the input layer pass on to the hidden layer its respective component of the feature vector obtained from the contour representation computed with the integral geometry-based functions (see Section III-B). In each neuron of the hidden layer, values that go to the next layer are transformed by evaluating a ReLU activation function. The values emitted by the output layer are processed by the softmax function to map the non-normalized output of a network to a probability distribution over predicted output classes. We perform the optimization of the cross-entropy loss function by adjusting the values of the connections (weights) between neurons using the backpropagation training process. This process applies a weight correction to reduce the difference between the network outputs and the desired ones so that the network can learn and reduce future errors.

E. Computational Cost

The computational cost and total memory required for calculating the feature vectors presented in Section II-C are related to the amount of information handled by the respective integral geometry-based function. As discussed by Herold-Garcia and Fernandes [17], the functions $p_\Phi(\sigma,\phi)$ and $\sigma_\Phi(p,\phi)$ consider only a tiny subset Φ of angular values, while $W(\phi)$, $W_c(\phi)$ and $C_\rho(\phi)$ use 360 angles to obtain the descriptor's map from which feature vectors are calculated. As a result, the computational cost and memory footprint of $p_\Phi(\sigma,\phi)$ and $\sigma_\Phi(p,\phi)$ are considerably lower than previous approaches. It is about 2% of the cost for the Φ set assumed in [17] and in our experiments.

It is well-known that the time complexity of the brute-force KNN classifiers to find the closest neighbor is $O(nd)$, where n is the number of classes and d the dimensionality of the feature [21]. Because there are few classes in erythrocyte shape classification problem (only three), in practice it is not worth organizing the data after model training in a tree to reduce such time complexity to something in the order of $O(\log(n)d)$.

For the ANN used in this work, the temporal complexity is $O((d+n)k)$, where where n is the number of classes, d the dimensionality of the feature, and k is the number of neurons in the hidden layer. Since $(n+n)k$ is much greater than nd, it turns out that the KNN classifier is the least complex alternative. However, the ANNs evaluated in our experiments are not prohibitive in terms of computational cost. Besides, they return better results in the classification.

III. Results and Discussions

This section compares the classification performance of the proposed method with previous integral geometry-based solutions where a KNN classifier was employed. Refer to [16], [17] and [20] for a comparison of state-of-the-art solutions to previous approaches from the literature.

A. Image Database

We have used the *erythrocytesIDB* image database [22], which consists of 202 images of normal cells, 210 images of sickle cells, and 213 images of cells with other deformations. The latter group includes images having shapes close to normal or sickle forms, making the classification of this class a challenging task. This is the same image database used in the investigations carried out with the original functions and their variants for computational cost reduction, *e.g.,* [16], [17], [20]. Fig. 1 shows some examples of images included in the *erythrocytesIDB* image database and the contour of their respective cells (in blue).

B. Feature Extraction

In all experiments that follow, we have considered the same parameterization as Gual-Arnau *et al.* [16], Herold-Garcia and Fernandes [17], and Gual *et al.* [20] to compute the descriptor functions: $\Delta\sigma = 1$, $\Delta p = 1$, $\Delta\phi = 1^\circ$ for $W(\phi)$ (2) and $C_\rho(\phi)$ (4); 8 values for σ in $W_c(\phi)$ (5); 8 values for ρ in $C_\rho(\phi)$ (4); and for the two other efficient descriptors, $p_\Phi(\sigma,\phi)$ (6) and $\sigma_\Phi(p,\phi)$ (7), we have considered the values $n = 8$ as the number of angles and $\phi_0 = 0$ in (8).

The Fourier coefficients used in the calculation of the feature vectors were taken as described in Section II-C. Still, experiments were carried out using a higher number of coefficients,

TABLE I
ANN HYPERPARAMETES (1ST EXPERIMENT)

	d	h	m	**Ep**	**Lr**	**Rg**
$W(\phi)$	7	70	3	1000	0.08	0.0
$C_\rho(\phi)$	7	90	3	1000	0.04	0.0
$W_c(\phi)$	6	80	3	1000	0.04	0.0008
$p_\Phi(\sigma,\phi)$	20	80	3	1000	0.2	0.0
$\sigma_\Phi(p,\phi)$	30	90	3	1000	0.01	0.0002

Hyperparameters: (d) Neurons in the input layer; (h) Neurons in the hidden layer; (m) Neurons in the output layer; (Ep) Epochs; (Lr) Learning rate; (Rg) Regularization

TABLE II
ANN HYPERPARAMETES (2ND EXPERIMENT)

	d	h	m	**Ep**	**Lr**	**Rg**
$W(\phi)$	6	50	3	1000	0.04	0.0
$C_\rho(\phi)$	6	30	3	1000	0.1	0.0
$W_c(\phi)$	8	30	3	1000	0.04	0.0001
$p_\Phi(\sigma,\phi)$	30	70	3	1000	0.008	0.004
$\sigma_\Phi(p,\phi)$	10	55	3	1000	0.01	0.0

Hyperparameters: (d) Neurons in the input layer; (h) Neurons in the hidden layer; (m) Neurons in the output layer; (Ep) Epochs; (Lr) Learning rate; (Rg) Regularization

especially for descriptors designed for reducing computational cost, due to the smaller amount of information they handle.

C. Experiments

We have performed three experiments to assess the performance of the proposed approach on the classification of erythrocytes in *normal*, *sickle* and *other deformation* classes:

- **1st experiment.** Following the methodology of previous works, in this experiment, we performed 5×1 cross-validation to obtain erythrocytes supervised classification and compared the results of our approach to results of state-of-the-art integral geometry-based techniques. Here, we randomly distributed the images in the folds while keeping the approximately uniform distribution of class samples in each of them.
- **2nd experiment.** In this experiment, we analyzed the response of the ANN-based classification models to elements that did not participate in the training/validation stage by considering 80% of the image database's entries for training/validation and 20% for model testing afterward. We applied 5×1 cross-validation during the training/validation stage, and we also randomly distributed the images in the partitions while keeping the approximately uniform distribution of class samples in each of them.
- **3rd experiment.** Here, we took the model with the best performance in the 2nd experiment and repeated the experiment considering different compositions for partitions to check the influence of the partition in the classification.

The selection of hyperparameters values for each ANN model in the 1st and 2nd experiments was performed by empirically exploring the space of hyperparameters. Tables I and II present the values that led to the best results for each descriptor function. The hyperparameters values set for the 2nd experiment were also used in the 3rd experiment.

The performance of the compared techniques was assessed considering recall (Rec), precision (Pre), F_1-score (F_1), and accuracy (Acc). Tables III and IV show all these values for, respectively, ANN and KNN classifiers in the 1st experiment. In the case of the $W(\phi)$ function, F_1-score values of 96.80%, 97.87% and 94.76% are reached in the *normal*, *sickle* and *other deformation* classes, respectively, with the use of ANN. This result is slightly lower than the one obtained previously using KNN for the case of the *normal* class (97.52%), and higher than the ones obtained for *sickle* and *other deformations* classes (96.42% and 94.14%, respectively). The accuracy achieved by the function $W(\phi)$ through the use of the ANN classifier (96.48%) is higher than the accuracy obtained with the use of the KNN method (96.00%).

With the descriptor $C_\rho(\phi)$, the use of ANN reached F_1-score values of 97.29%, 96.71%, and 94.01% for the *normal*, *sickle*, and *other deformations* classes, respectively. This result is higher than the one achieved using the KNN algorithm in the *sickle* class (96.24%), and slightly lower than those achieved for *normal* and *other deformations* classes. In both cases the accuracy is similar, 96% and 96.16%, respectively.

TABLE III
CONFUSION MATRIX AND PERFORMANCE OF ALL DESCRIPTORS USING ANN CLASSIFIERS (1ST EXPERIMENT)

		N	S	O	Rec	Pre	F_1	Acc
$W(\phi)$	**N**	197	0	5	97.52	96.10	96.80	
	S	0	207	3	98.57	97.18	97.87	96.48
	O	8	6	199	93.43	96.14	94.76	
		N	**S**	**O**	**Rec**	**Pre**	**F_1**	**Acc**
$C_\rho(\phi)$	**N**	198	0	4	98.02	96.59	97.29	
	S	0	206	4	98.10	95.37	96.71	96.00
	O	7	10	196	92.02	96.08	94.01	
		N	**S**	**O**	**Rec**	**Pre**	**F_1**	**Acc**
$W_c(\phi)$	**N**	197	0	5	97.52	95.16	96.33	
	S	0	207	3	98.57	97.18	97.87	96.16
	O	10	6	197	92.49	96.10	94.25	
		N	**S**	**O**	**Rec**	**Pre**	**F_1**	**Acc**
$p_\Phi(\sigma,\phi)$	**N**	199	0	3	98.51	95.67	97.07	
	S	0	205	5	97.62	97.16	97.38	96.32
	O	9	6	198	92.96	96.12	94.51	
		N	**S**	**O**	**Rec**	**Pre**	**F_1**	**Acc**
$\sigma_\Phi(p,\phi)$	**N**	199	0	3	98.51	96.60	97.55	
	S	0	208	2	99.05	97.20	98.11	97.12
	O	7	6	200	93.90	97.56	95.69	

Classes: (N) Normal; (S) Sickle; (O) Other deformations
Metrics: (Rec) Recall; (Pre) Precision; (F_1) F_1-score; (Acc) Accuracy

TABLE IV
CONFUSION MATRIX AND PERFORMANCE OF ALL DESCRIPTORS USING KNN CLASSIFIERS (1ST EXPERIMENT)

		N	S	O	Rec	Pre	F_1	Acc
$W(\phi)$	**N**	197	0	5	97.52	97.52	97.52	
	S	0	202	8	96.19	96.65	96.42	96.00
	O	5	7	201	94.37	93.93	94.14	
		N	**S**	**O**	**Rec**	**Pre**	**F_1**	**Acc**
$C_\rho(\phi)$	**N**	198	0	4	98.02	98.02	98.02	
	S	0	205	5	97.62	94.91	96.24	96.16
	O	4	11	198	92.96	95.65	94.28	
		N	**S**	**O**	**Rec**	**Pre**	**F_1**	**Acc**
$W_c(\phi)$	**N**	195	0	7	96.53	93.75	95.12	
	S	0	202	8	96.19	95.28	95.73	93.92
	O	13	10	190	89.20	92.68	90.91	
		N	**S**	**O**	**Rec**	**Pre**	**F_1**	**Acc**
$p_\Phi(\sigma,\phi)$	**N**	195	0	7	96.53	95.59	96.06	
	S	0	201	9	95.71	96.17	95.94	94.72
	O	9	8	196	92.02	92.45	92.23	
		N	**S**	**O**	**Rec**	**Pre**	**F_1**	**Acc**
$\sigma_\Phi(p,\phi)$	**N**	197	0	5	97.52	95.17	96.33	
	S	0	199	11	94.76	94.76	94.76	94.08
	O	10	11	192	90.14	92.31	91.21	

Classes: (N) Normal; (S) Sickle; (O) Other deformations
Metrics: (Rec) Recall; (Pre) Precision; (F_1) F_1-score; (Acc) Accuracy

In the cases of the functions tailored for reducing computational cost ($W_c(\phi)$, $p_\Phi(\sigma,\phi)$, and $\sigma_\Phi(p,\phi)$), the accuracy values achieved using ANN were 96.16%, 96.32%, and 97.12%, respectively, which are higher than the accuracies 93.92%, 94.72%, and 94.08% obtained using the KNN classifier, and also equivalent or better than those obtained using the original functions ($W(\phi)$ and $C_\rho(\phi)$) with the KNN classifier. These are excellent results, especially considering the high degree of computational cost reduction that these functions provide, especially $p_\Phi(\sigma,\phi)$ and $\sigma_\Phi(p,\phi)$. With this, we demonstrate

that ANN models trained with the analyzed descriptors achieve better results than KNN-based classification algorithm. Hence, with ANN, the representation potentialities of these descriptors are better exploited.

Tables V and VI show the results obtained in the 2nd experiment. Recall that this experiment considers 80% of the images for the ANN models' training and validation, while the remaining 20% is used to test the models. This experiment allows us to analyze the real capacity of generalization that the ANN has when classifying elements that do not participate in the training/validation and model selection stage.

In the training/validation stage (Table V), the accuracy values are high, all over 95%, which shows the learning capacity of the model trained with the integral geometry-based characteristics. The most interesting results are obtained in the testing stage of the model (Table VI), where all the functions have accuracy values higher than 95%, too. For the function $C_\rho(\phi)$, the value obtained (95.20%) does not exceed that reached using the KNN classifier, which was 96.15% in the 1st experiment, but for the other functions, the accuracy values reached using ANN are higher. The case with the best result is the combination of $\sigma_\Phi(p,\phi)$ with the ANN classifier, whose accuracy is 98.40%.

In the last experiment, we repeated the 2nd experiment three more times for the best-rated descriptor using a different set of images in each partition to verify the influence that the composition of the training/validation and testing data may have on learning the ANN parameters/weights using 80% of the data and classifying the remaining 20% of the images. Table VII summarizes the performances achieved by combining the $\sigma_\Phi(p,\phi)$ function with the ANN classifier in the 3rd experiment. Notice that the accuracy is greater than 96% in all cases. These results show that for an image database such as the *erythrocytesIDB* [22], the partitioning of the universe used for carrying out the training/validation of the ANN model does not have much influence on the final result, and the $\sigma_\Phi(p,\phi)$-based descriptor provides better accuracy results than using KNN with any of the analyzed functions.

From a practical point of view, a predictive model is exposed to two types of errors: false positives (FP, or type I error) and false negatives (FN, or type II error). Depending on the nature of the problem, a model that makes fewer errors of one or both types is of greater interest. In this case, for the clinical follow-up of the patient with sickle cell anemia disease, the possibility of a crisis is determined fundamentally by the existence of sickle cells, so this is the class of most significant interest to study, and both scenarios are important. Therefore, an automated method to evaluate the patient's condition should minimize the occurrence of both types of errors, both FP and FN, in the sickle cell class (it means F_1-score is maximized in this class). It is because when the model does not classify as sickle those erythrocytes that belong to that class, it will not allow the correct analysis of the cell deformation. As a result, the incorrect classification may lead to a wrong diagnosis of a possible crisis, and the patient would not receive the appropriate treatment. In the opposite case, an automated model that classifies as sickle those erythrocytes that do not belong to that class may induce the specialist to consider the proximity of a crisis and the treatment will be indicated to the patient unnecessarily, which in the same way is not recommended. Thus, both errors should be considered when evaluating the models.

On model testing, the functions $W(\phi)$ and $\sigma_\Phi(p,\phi)$ show the best results of F_1-score in the sickle cell class with 100% (Table VI). Besides, the other two descriptors that guarantee the reduction of the computational cost to obtain

TABLE V
CONFUSION MATRIX AND PERFORMANCE OF ALL DESCRIPTORS ON MODEL TRAINING/VALIDATION USING ANN CLASSIFIERS (2ND EXPERIMENT)

		N	S	O	Rec	Pre	F_1	Acc
$W(\phi)$	**N**	159	0	2	98.76	95.78	97.24	
	S	0	168	3	98.25	96.55	97.39	96.39
	O	7	6	154	92.22	96.86	94.47	
		N	**S**	**O**	**Rec**	**Pre**	F_1	**Acc**
$C_\rho(\phi)$	**N**	157	0	4	97.52	93.45	95.44	
	S	0	167	4	97.66	97.09	97.37	95.22
	O	11	5	151	90.59	95.06	92.77	
		N	**S**	**O**	**Rec**	**Pre**	F_1	**Acc**
$W_c(\phi)$	**N**	159	0	2	98.76	95.21	96.95	
	S	0	165	6	96.49	97.06	96.77	95.79
	O	8	5	154	92.22	95.06	93.61	
		N	**S**	**O**	**Rec**	**Pre**	F_1	**Acc**
$p_\Phi(\sigma,\phi)$	**N**	159	0	2	98.76	96.36	97.54	
	S	0	169	2	98.83	95.48	97.12	96.39
	O	6	8	153	91.62	97.45	94.44	
		N	**S**	**O**	**Rec**	**Pre**	F_1	**Acc**
$\sigma_\Phi(p,\phi)$	**N**	157	0	4	97.51	96.31	96.91	
	S	0	165	6	96.49	96.49	96.49	95.59
	O	6	6	155	92.81	93.93	93.37	

Classes: (N) Normal; (S) Sickle; (O) Other deformations
Metrics: (Rec) Recall; (Pre) Precision; (F_1) F_1-score; (Acc) Accuracy

TABLE VI
CONFUSION MATRIX AND PERFORMANCE OF ALL DESCRIPTORS ON MODEL TESTING USING ANN CLASSIFIERS (2ND EXPERIMENT)

		N	S	O	Rec	Pre	F_1	Acc
$W(\phi)$	**N**	38	0	2	95.00	95.00	95.00	
	S	0	39	0	100.0	100.0	100.0	96.80
	O	2	0	44	95.65	95.65	95.65	
		N	**S**	**O**	**Rec**	**Pre**	F_1	**Acc**
$C_\rho(\phi)$	**N**	39	0	1	97.50	95.12	96.29	
	S	0	37	2	94.87	97.37	96.10	95.20
	O	2	1	43	93.48	93.48	93.48	
		N	**S**	**O**	**Rec**	**Pre**	F_1	**Acc**
$W_c(\phi)$	**N**	38	0	2	95.00	92.68	93.83	
	S	0	38	1	97.44	100.0	98.70	95.20
	O	3	0	43	93.48	93.48	93.48	
		N	**S**	**O**	**Rec**	**Pre**	F_1	**Acc**
$p_\Phi(\sigma,\phi)$	**N**	39	0	1	97.50	95.12	96.29	
	S	0	38	1	97.44	100.0	98.70	96.80
	O	2	0	44	95.65	95.65	95.65	
		N	**S**	**O**	**Rec**	**Pre**	F_1	**Acc**
$\sigma_\Phi(p,\phi)$	**N**	40	0	0	100.0	95.23	97.56	
	S	0	39	0	100.0	100.0	100.0	98.40
	O	2	0	44	95.65	100.0	97.77	

Classes: (N) Normal; (S) Sickle; (O) Other deformations
Metrics: (Rec) Recall; (Pre) Precision; (F_1) F_1-score; (Acc) Accuracy

the characteristics reached a value of 98.70% for F_1-score in sickle cell class, which is also very high. Hence, it is valid to consider the optimized functions instead of the original ones. Performing an analysis within each class for the case of the descriptor that obtains the best result, $\sigma_\Phi(p,\phi)$, it is found that it considerably improves classification performance when used with an ANN-model, reaching values of F_1-score of 97.56%, 100% and 97.77% for the *normal*, *sickle* and *other deformations* classes in the 2nd experiment (Table VI) and 97.55%, 98.11% and 95.69% in the 1st experiment (Table III). These results are much higher than those reached when the same descriptor was used with a KNN classifier (96.33%, 94.76% and 91.21% in Table IV). This confirms that the use of the characteristics obtained with these integral geometry-based functions to train a model of ANN allows to improve the performance reported so far in the literature, by reducing the number of cases that were not correctly predicted by the KNN classifier in the classes of greatest interest, *i.e., sickle* and *other deformations*, where there are elements with shapes similar to normal and sickle, which in turn allowed to improve the performance in the class of *normal* cells.

It is important to comment that the variations on the F_1-scores and accuracy values presented for $\sigma_\Phi(p,\phi)$ in the last rows of Table VI and in Table VII occur due to the database's characteristics, where some of the elements of the class *other deformations* are similar to the *sickle* and *normal* shape classes. So, it is natural that some partitions lead to better results than others, according to their composition. It is worth noting that with all partitions tested with ANN, the results obtained are better than with KNN, which illustrates the stability of the proposed technique.

The performances reported in this work are better than those for previous integral geometry-based solutions where KNN was employed and reached values equal to or better than the performance reported by other recent approaches. Recall that the potential of these functions have been demonstrated under similarity conditions between objects of different classes, while the majority of previous works have studied classes of well-differentiated object.

The $\sigma_\Phi(p,\phi)$ is one of the functions that allow the reduction of the computational effort of the original functions (reduction of $\sim 98\%$ [17]). At the same time, it presents a high F_1-score when combined with ANN-based classifiers, and automated methods to evaluate the patient's condition should maximize the F_1-score for the *sickle* and *other deformation* classes. These results suggest that our approach has the desired properties to be implemented in mobile apps designed as self-awareness tools to facilitate the analysis of blood smears of individuals with sickle cell disease or screening in developing countries where specialists might not be available. As future work, we will investigate how the accuracy of the proposed technique for classification of red blood cells' shape impacts the quality of peripheral blood smear analysis to support the medical follow-up diagnosis of sickle cell disease. But for that, it will be necessary to have access to a dataset that relates the blood samples to the patient's diagnosis.

TABLE VII
PERFORMANCE OF THE $\sigma_\Phi(p,\phi)$ DESCRIPTOR ON MODEL TESTING USING ANN CLASSIFIERS AND CONSIDERING OTHER PARTITIONINGS (3RD EXPERIMENT)

Partitioning #	Class	Rec	Pre	F_1	Acc
1	**N**	100.0	97.56	98.76	98.40
	S	97.44	100.0	98.70	
	O	97.83	97.83	97.83	
2	**N**	100.0	95.45	97.67	96.80
	S	95.55	100.00	97.72	
	O	94.74	94.74	94.74	
3	**N**	97.37	97.37	97.33	96.20
	S	97.78	95.65	96.99	
	O	92.86	95.12	93.49	

Classes: (N) Normal; (S) Sickle; (O) Other deformations
Metrics: (Rec) Recall; (Pre) Precision; (F_1) F_1-score; (Acc) Accuracy

IV. CONCLUSION

We presented a new approach for the morphological classification of erythrocytes that combines features obtained from the functional representation of the red blood cells contour using integral geometry-based functions and an ANN-based classifier. We carried out a comparative study of this approach and state-of-the-art solutions based on integral geometry-based functions where KNN was used. Results show that, with the functions $W_c(\phi)$, $p_\Phi(\sigma,\phi)$, $\sigma_\Phi(p,\phi)$, *i.e.,* the variants of the original functions that allow the reduction of the computational cost, 95.20%, 96.80% and 96.20%-98.40% of accuracy were reached (recall that in the case of the $p_\Phi(\sigma,\phi)$ function, the experiments were realized at least four times with different partitions). Those results outperform previous works that consider the same set of classes for red blood cell's shape. Those techniques achieved, respectively, 93.92%, 94.72%, and 94.08% of accuracy by assuming a KNN-based classifier. For the case of the descriptor $\sigma_\Phi(p,\phi)$ combined with an ANN-based classifier, the solution with better results, our experiments reported that the F_1-score of the *sickle* and *other deformations* classes were 96.99%-100% and 93.49%-97.83%, respectively, and reduction of confusion cases between classes was achieved. The same function with KNN achieved F_1-scores of 94.76% and 91.21%, respectively.

It is important to emphasize that the integral geometry-based features used in this research do not require data augmentation while training our ANN-based classifier since these features are invariant to rotation, translation, and scale.

ACKNOWLEDGMENT

The authors would like to thank: Belgium Development Cooperation through VLIR-UOS (Flemish Interuniversity Council – University Cooperation for Development) within the IUC Universidad de Oriente Program; Project PT241SC003-006 of the CITMA Santiago Delegation Territorial Program for Development of Health Products and Services 2020; Institutional Project 0125 of Universidad de Guantánamo; CNPq-Brazil (grant 311.037/2017-8); and FAPERJ (grant E-26/202.718/2018).

REFERENCES

[1] D. Manwani and P. S. Frenette, "Vaso-occlusion in sickle cell disease: pathophysiology and novel targeted therapies," *The Journal of the American Society of Hematology*, vol. 24, no. 122, pp. 3892–3898, 2013.

[2] World Health Organization. Sickle cell disease. [Online]. Available: https://www.afro.who.int/health-topics/sickle-cell-disease

[3] B. Marcheco-Teruel, "Sickle cell anemia in Cuba: prevention and management, 1982-2018," *MEDICC Review*, vol. 21, no. 4, pp. 34–38, 2019.

[4] Ministério da Saúde. Anemia falciforme. In Portuguese. [Online]. Available: https://bvsms.saude.gov.br/dicas-em-saude/437-anemia-falciforme

[5] Z. M. Abood, G. S. Karam, and R. E. Hluot, "Classification of red blood cells disease using fuzzy logic theory," in *Proceedings of the International Conference on Current Research in Computer Science and Information Technology (ICCIT)*, 2017, pp. 31–36.

[6] N. Safca, D. Popescu, L. Ichim, H. Elkhatib, and O. Chenaru, "Image processing techniques to identify red blood cells," in *Proceedings of the 22nd International Conference on System Theory, Control and Computing (ICSTCC)*, 2017, pp. 93–986.

[7] W. Delgado-Font, M. Escobedo-Nicot, M. González-Hidalgo, S. Herold-Garcia, A. Jaume-i Capó, and A. Mir, "Diagnosis support of sickle cell anemia by classifying red blood cell shape in peripheral blood images," *Medical & Biological Engineering & Computing*, vol. 58, no. 6, pp. 1265–1284, 2020.

[8] T. S. Chy and M. A. Rahaman, "Automatic sickle cell anemia detection using image processing technique," in *Proceedings of the International Conference on Advancement in Electrical and Electronic Engineering (ICAEEE)*, 2018, pp. 1–4.

[9] J. A. Alkrimi, S. A. Tome, and E. George, "Classification of red blood cells using principal component analysis technique," *European Journal of Engineering Research and Science*, vol. 4, no. 2, pp. 17–22, 2019.

[10] Z. Alom, C. Yakopcic, T. M. Taha, and V. K. Asari, "Microscopic blood cell classification using inception recurrent residual convolutional neural networks," in *Proceedings of the IEEE National Aerospace and Electronics Conference (NAECON)*, 2018, pp. 222–227.

[11] M. Grochowski, M. Wasowicz, A. Mikołajczyk, M. Ficek, M. Kulka, M. S. Wróbel, and M. Jedrzejewska-Szczerska, "Machine learning system for automated blood smear analysis," *Metrology and Measurement Systems*, vol. 26, no. 1, pp. 81–93, 2019.

[12] H. A. Elsalamony, "Detecting distorted and benign blood cells using the hough transform based on neural networks and decision trees," in *Emerging Trends in Image Processing, Computer Vision and Pattern Recognition*. Morgan Kaufmann, 2015, pp. 457–473.

[13] D. A. Tyas, T. Ratnaningsih, A. Harjoko, and S. Hartati, "The classification of abnormal red blood cell on the minor thalassemia case using artificial neural network and convolutional neural network," in *Proceedings of the International Conference on Video and Image Processing (ICVIP)*, 2017, pp. 228–233.

[14] D. Frejlichowski, "Pre-processing, extraction and recognition of binary erythrocyte shapes for computer-assisted diagnosis based on MGG images," in *Proceedings of the International Conference on Computer Vision and Graphics (ICCVG) – LNCS*, vol. 6374, 2010, pp. 368–375.

[15] W. Delgado-Font, M. González-Hidalgo, S. Herold-Garcia, A. Jaume-i Capó, and A. Mir, "Erythrocytes morphological classification through HMM for sickle cell detection," in *Proceedings of the International Conference on Articulated Motion and Deformable Objects – LNCS*, vol. 9756, 2016, pp. 88–97.

[16] X. Gual-Arnau, S. Herold-Garcia, and A. Simo, "Erythrocyte shape classification using integral geometry-based methods," *Medical & Biological Engineering & Computing*, vol. 7, no. 53, pp. 623–633, 2015.

[17] S. Herold-Garcia and L. A. F. Fernandes, "New methods for morphological erythrocytes classification," in *Proceedings of the 41st Annual International Conference of the IEEE Engineering in Medicine and Biology Society (EMBC)*, 2019, pp. 4068–4071.

[18] X. Gual-Arnau, S. Herold-Garcia, and A. Simó, "Geometric analysis of planar shapes with applications to cell deformation," *Image Analysis & Stereology*, vol. 34, no. 3, pp. 171–182, 2015.

[19] I. Epifanio, X. Gual-Arnau, and S. Herold-Garcia, "Morphological analysis of cells by means of an elastic metric in the shape space," *Image Analysis & Stereology*, vol. 39, no. 1, pp. 281–291, 2020.

[20] X. Gual, S. Herold, and A. Simó, "Shape description from generalized support functions," *Pattern Recognition Letters*, vol. 34, no. 6, pp. 619–626, 2013.

[21] F. P. Preparata and M. I. Shamos, *Computational geometry: an introduction*. Berlin, Heidelberg: Springer-Verlag, 1985.

[22] M. González-Hidalgo, F. A. Guerrero-Peña, S. Herold-García, A. Jaume-i Capó, and P. D. Marrero-Fernández, "Red blood cell cluster separation from digital images for use in sickle cell disease," *IEEE Journal of Biomedical and Health Informatics*, vol. 19, no. 4, pp. 1514–1525, 2015.